AMERICAN ACADEMY OF OPHTHALMOLOGY®

Retinitis Punctata Albescens and *RLBP1*-Allied Phenotypes

Phenotype–Genotype Correlation and Natural History in the Aim of Gene Therapy

Béatrice Bocquet, PhD,[1,2] Hicham El Alami Trebki, MD,[1] Anne Françoise Roux, PharmD, PhD,[2,3] Gilles Labesse, PhD,[4] Philippe Brabet, PhD,[2] Carl Arndt, MD, PhD,[5] Xavier Zanlonghi, MD,[6] Sabine Defoort-Dhellemmes, MD,[7] Dalil Hamroun, PhD,[8] Céline Boulicot-Séguin, MD,[9] Léopoldine Lequeux, MD,[10] Marie Christine Picot, MD,[11] Hélèna Huguet,[11] Isabelle Audo, MD, PhD,[12] Claire Marie Dhaenens, PharmD, PhD,[13] Vasiliki Kalatzis, PhD,[2] Isabelle Meunier, MD, PhD[1,2]

Purpose: To identify relevant criteria for gene therapy based on clinical and genetic characteristics of rod–cone dystrophy associated with *RLBP1* pathogenic variants in a large cohort comprising children and adults.

Design: Retrospective cohort study.

Participants: Patients with pathogenic variants in *RLBP1* registered in a single French reference center specialized in inherited retinal dystrophies.

Methods: Clinical, multimodal imaging, and genetic findings were reviewed.

Main Outcome Measures: Age of onset; visual acuity; ellipsoid line length; nasal, temporal, and foveal retinal thickness; and pathogenic variants and related phenotypes, including Newfoundland rod–cone and Bothnia dystrophies (NFRCDs), were reappraised.

Results: Twenty-one patients (15 families) were included. The most frequent form was NFRCD with 12 patients (8 families) homozygous for the recurrent deletion of exons 7 through 9 in *RLBP1* and 5 patients (4 families) with biallelic protein-truncating variants (2 novel: p.Gln16* and p.Tyr251*). A novel combination of the p.Arg234Trp Bothnia variant with a nonsense variant in *trans* led to Bothnia dystrophy in 2 sisters. One proband carrying the p.Met266Lys Bothnia variant and in *trans* p.Arg121Trp and a second, with the p.Arg9Cys and p.Tyr111* combination, both demonstrated mild retinitis punctata albescens. Independently of genotype, all patients showed a visual acuity of worse than 20/200, an ellipsoid line width of less than 1000 μm, and a mean foveal thickness of less than 130 to 150 μm, with loss of both the interdigitation and ellipsoid lines.

Conclusions: The eligibility for *RLBP1* gene therapy first should be determined according to the biallelic variant combination using a robust classification as proposed herein. An ellipsoid line width of more than 1200 μm and a central thickness of more than 130 to 150 μm with detectable ellipsoid and interdigitation lines should be 2 prerequisite imaging indicators for gene therapy. *Ophthalmology Science 2021;1:100052*

Retinitis punctata albescens (RPA) is an autosomal recessive rod–cone dystrophy (RCD) recognizable by numerous small and round white dots scattered throughout the posterior pole and peripheral retina at initial stages and by the occurrence of peripheral atrophic patches at later stages. Retinitis punctata albescens is rare and accounts for approximately 1% of patients with autosomal recessive RCD (1/800 000 individuals worldwide).[1] Retinitis punctata albescens is associated with a relatively long-term preservation of the macular zone and visual acuity, except in 2 severe RPA subtypes, Bothnia dystrophy (BD) and Newfoundland RCD (NFRCD).[2,3] Bothnia dystrophy, so named because of its high prevalence in Bothnia, a northern area of Sweden, differs by an early atrophic maculopathy that occurs during the second or third decade of life. Newfoundland RCD, with a high prevalence in Newfoundland, Canada, presents as a rapid form of RCD leading to legal blindness during the third decade of life.

All 3 phenotypes of RPA are caused by biallelic variations in the *RLBP1* gene (Online Mendelian Inheritance in Man identifier, 180090). *RLBP1*, located on chromosome 15q26.1, expresses a 1.752-kb transcript that encodes the cellular retinaldehyde-binding protein (CRALBP; 36 kDa; 317 aa; UniProtKB identifier, P12271) that is a member of the CRAL-TRIO protein superfamily. Cellular retinaldehyde-binding protein expression and function were

https://doi.org/10.1016/j.xops.2021.100052
ISSN 2666-9145/21

demonstrated both in retinal pigment epithelium (RPE) and Müller cells. This protein plays a key role in the visual cycle that ensures the renewal of the 11 cis-retinal required for phototransduction in the photoreceptors.[4] It also plays a role in cone visual function and the associated visual cycle of Müller cells.[5] Forty-two *RLBP1* pathogenic variants have been reported to date in the literature and the Human Gene Mutation Database (HGMD) professional database (accessed April 1, 2021), comprising 18 insertions and deletions, 17 missense, 3 nonsense, and 4 splicing variations.[1–4,6–21] Recurrent deletions with founder effects also have been reported, particularly in Mediterranean populations. One novel large deletion not reported in HGMD recently was identified in 1 patient.[22] To date, only 2 specific missense pathogenic variants, p.Arg234Trp and p.Met226Lys, have been associated with BD, and 3 splicing variants, predicted to lead to the lack of a functional protein, have been associated with NFRCD.[3,6]

Because an *RLBP1* gene therapy clinical trial is currently ongoing (ClinicalTrials.gov identifier, NCT03374657), it is of great importance to define pertinent gene therapy eligibility criteria. For this purpose, we reviewed the clinical and genetic data of 21 patients (15 families) carrying biallelic pathogenic variants in *RLBP1* followed up in our reference center specialized in inherited retinal dystrophies (IRDs). We herein reappraised variant combinations and their corresponding clinical phenotypes, as well as the lower limiting values of macular thicknesses and ellipsoid line widths, to define patient eligibility for gene therapy.

Methods

All patients with biallelic pathogenic variants in *RLBP1* were recruited from the patient database of a national French reference center dedicated to IRDs. Signed informed consent for clinical examination and genetic analysis was obtained. All methods were carried out in accordance with approved protocols of the Montpellier University Hospital and in agreement with the tenets of the Declaration of Helsinki. The Ministry of Public Health accorded approval for biomedical research under the authorization number 11018S.

Clinical Investigation

Age at onset, initial symptoms, best-corrected visual acuity measured with Snellen charts, Goldmann visual field (GVF), electroretinography, infrared and fundus autofluorescence imaging, and macular spectral-domain (SD) OCT scans were reviewed. Color photographs were obtained with a nonmydriatic automated fundus camera (AFC 330; Nidek, Inc). Fundus autofluorescence and SD OCT imaging were completed with a combined Heidelberg Retina Angiograph + Spectralis OCT device (Heidelberg Engineering). To confirm RCD, full-field electroretinography was performed with a contact lens electrode using a Ganzfeld apparatus (Ophthalmologic Monitor Metrovision) according to the guidelines of the International Society for Electrophysiology of Vision. Goldmann visual fields were classified based on the criteria of the World Health Organization (mild visual impairment for a central visual field between 20° and 70°, low vision if limited to the central 20°, and blindness if inferior to 10°).

On SD OCT scans, central foveal thickness was measured independently in each eye with automated segmentation Heidelberg Eye Explorer (HEYEX) software (Heidelberg Engineering). Retinal thickness, defined as the distance between the basal RPE–Bruch's membrane and the internal limiting membrane, were measured at the fovea, at 1500 μm and 3000 μm nasal to the fovea, and at 1500 μm and 3000 μm temporal to the fovea on the horizontal 30° section by the automated software and, if necessary, manually by 2 independent operators (X.Z., I.M.). The horizontal ellipsoid line width was measured on the horizontal 30° section by the 2 independent operators (X.Z., I.M.). The disease progression was assessed only in patients having undergone at least 2 examinations with SD OCT, available in our department from 2010.

Molecular Investigation

Genomic DNA was extracted from leukocytes using FlexiGene kit (Qiagen). DNA sequencing of the 9 exons (including flanking intronic sequences) of *RLBP1* was carried out using the BigDye Terminator Cycle Sequencing Ready Reaction kit version 3.1 (Applied Biosystems) on an ABI PRISM 3130 capillary sequencer (Applied Biosystems). Sequencing results were analyzed using SeqScape Software version 2.5 (Applied Biosystems; detailed procedure available on request). The homozygous exon 7 to 9 deletion was confirmed by the amplification of a 334-bp fragment after polymerase chain reaction analysis, using the primer pairs 5′-TTGGGAGAACTTTGGCATG-3′ and 5′-TGTGAAGCTGAGCACGTCAGAT-3′. The amplification of this fragment reflects the deletion of 7359 bp and the insertion of 1 bp, as described previously.[23]

Variant Analysis and Protein Modelling

Familial variant segregation analysis was carried out for each participant (at least 1 relative). Variant classification was assessed according to the American College of Medical Genetics and Genomics guidelines.[24] The possible impacts of novel missense variants were predicted by an *in silico* analysis using the databases Provean (Protein Variation Effect Analyzer, http://provean.jcvi.org), PolyPhen2 (Polymorphism Phenotyping 2, http://genetics.bwh.harvard.edu/pph2/index.shtml), Mutation taster (http://mutationtaster.org/), Mobidetails (https://mobidetails.iurc.montp.inserm.fr/MD/), and Varsome (https://varsome.com/). The protein sequence of the various mutants were submitted to the webserver @TOME for sequence-structure alignment and model building using SCWRL 3.0.[25,26] Resulting models were visualized and analyzed using Pymol (www.pymol.org).

Statistical Analyses

The study population was described with means and standard deviations or boxplots for quantitative variables and with frequencies for qualitative variables. Comparisons between eyes were performed using a paired Student *t* test when the distribution was Gaussian, or with a Wilcoxon signed-rank test for continuous data. Between phenotypes, the characteristics of the patients were compared using the Student *t* test when the distribution was Gaussian, or with the Mann–Whitney *U* test. For qualitative variables, groups were compared using the chi-square test or Fisher exact test. The same tests were used for comparisons between control participants and *RLBP1*-related patients. The comparison of eye characteristics between phenotypes was performed with a linear mixed model with a random effect for participant (to take into account the measurements on both eyes) and phenotypes and age as fixed effects. Tukey's correction was applied for pairwise comparisons. Pearson's or Spearman's coefficients were calculated to measure the correlation between parameters. The statistical significance was set at 0.05, and analyses were performed using

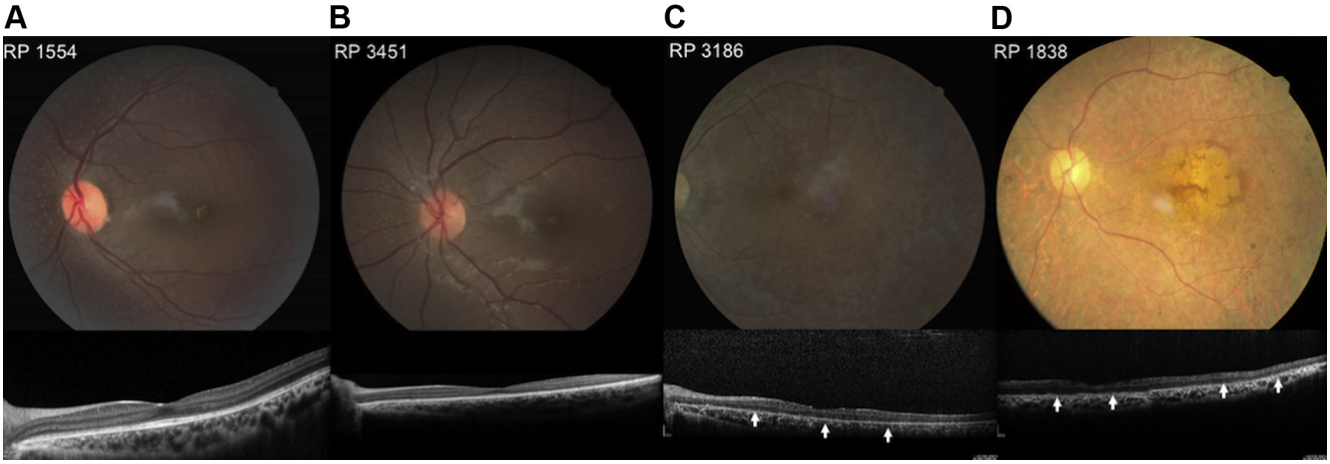

Figure 1. **A**–**D**, Newfoundland rod–cone dystrophy (top row) fundus photographs and (bottom row) spectral-domain (SD) OCT images from 4 patients (patients RP1554, RP3451, RP3186, and RP1838) showing a pattern from childhood to adulthood. **A**, **B**, Patients RP1554 and RP3451 were examined at the age of 10 years. Note that the white dots are more visible in the nasal retina. The retinal vessels are preserved. On SDOCT scans, already a retinal thinning is present, even in the foveal zone, for patient RP3451 and the ellipsoid line shows a granular appearance. **C**, **D**, Patients RP3186 (at 42 years of age) and RP1838 (at 31 years of age) with severe visual loss. SDOCT horizontal scans show the disappearance of the ellipsoid zone (arrows), interdigitation zone (IZ), and outer nuclear layer in these last 2 patients. Noted the narrowed retinal vessels, the papillary pallor, and the pigmentary changes in the mid periphery. Moreover, complete macular atrophy also occurred in both eyes of patient RP1838 after 30 years of age.

Statistical Analysis Systems Enterprise Guide software version 4.3 (SAS Institute).

Results

Overall, 21 patients from 15 families with biallelic variations in *RLBP1* were included in this study. We previously reported 11 of these 21 patients (8 families), but we did not delineate different clinical forms, nor focus on genotype–phenotype correlations.[7] Herein, based on genetic data, we determined that NFRCD was the most prevalent phenotype in the cohort, noted in 17 affected patients, whereas 2 patients demonstrated BD and 2 others, classic RPA.

Newfoundland Rod–Cone Dystrophy

All patients with NFRCD harbored large deletions or nonsense or frameshift variants in both alleles, which likely led to a complete absence of the encoded CRALBP and an NFRCD phenotype (Figs 1 and 2). All 12 Moroccan patients (8 families; patients RP517, RP702, RP1554, RP1633, RP1789, RP1838, RP3066, and RP3451) were homozygous for the recurrent *RLBP1* deletion of exons 7 through 9.[23] The Algerian patient (patient RP3186; Fig 2) carried a pathogenic homozygous frameshift variant, c.203del (p.Glu68Glyfs*51).[14] Regarding the White French patients, proband RP1682 was homozygous for the frameshift variant c.487dup (p.Ile163Asnfs*1).[21] The affected brothers from family RP2610 were compound heterozygous for a novel stop variant, c.46C>T (p.Gln16*) (not reported in the gnomAD database and predicted to be pathogenic according to American College of Medical Genetics 2015), in *trans* with the previously described nonsense variant c.466C>T (p.Arg156*).[11] Finally, the proband from the Madagascan family PB70 was homozygous for a novel stop variant, c.753C>A (p.Tyr251*), present in gnomAD at a frequency of 2.316e-5, never reported in the homozygous state, and classified as pathogenic according to the ACMG classification.[24]

Bothnia Dystrophy

The 2 French sisters (patients RP857-1 and RP857-2; Fig 3) with BD were compound heterozygous for the specific c.700C>T (p.Arg234Trp) Bothnia variant[6,7] in *trans* with the nonsense variant c.333T>G (p.Tyr111*) in exon 5. Because p.Tyr111* likely undergoes nonsense-mediated mRNA decay (NMD), the produced protein is coded only by the DNA c.700C>T allele, and thus leading to the severe Bothnia phenotype.

Classic Retinitis Punctata Albescens Phenotype

A first RPA patient (patient RP1254) was compound heterozygous for the c.25C>T (p.Arg9Cys) variant in exon 4 and the c.333T>G (p.Tyr111*) variant in exon 5.[7] Again, because p.Tyr111* likely undergoes NMD, the only protein produced would be encoded by the mutated allele c.333T>G. With regard to the structural models of CRALBP (Fig 4), the variant p.Arg9Cys is predicted to have a lower solubility, although it is predicted to adopt the same folding as the wild-type protein.[27] However, the mutation cannot be modeled precisely because it occurs in a region of the protein that is not seen in the 2 crystal structures of CRALBP.

The other unrelated RPA patient (patient RP2632; Fig 5) carried 2 biallelic missense variants, the novel c.361C>T (p.Arg121Trp) variant in *trans* with the c.677T>A (p.Met226Lys).[15] Although the p.Arg121Trp variant was classified as a variant of uncertain significance, it was

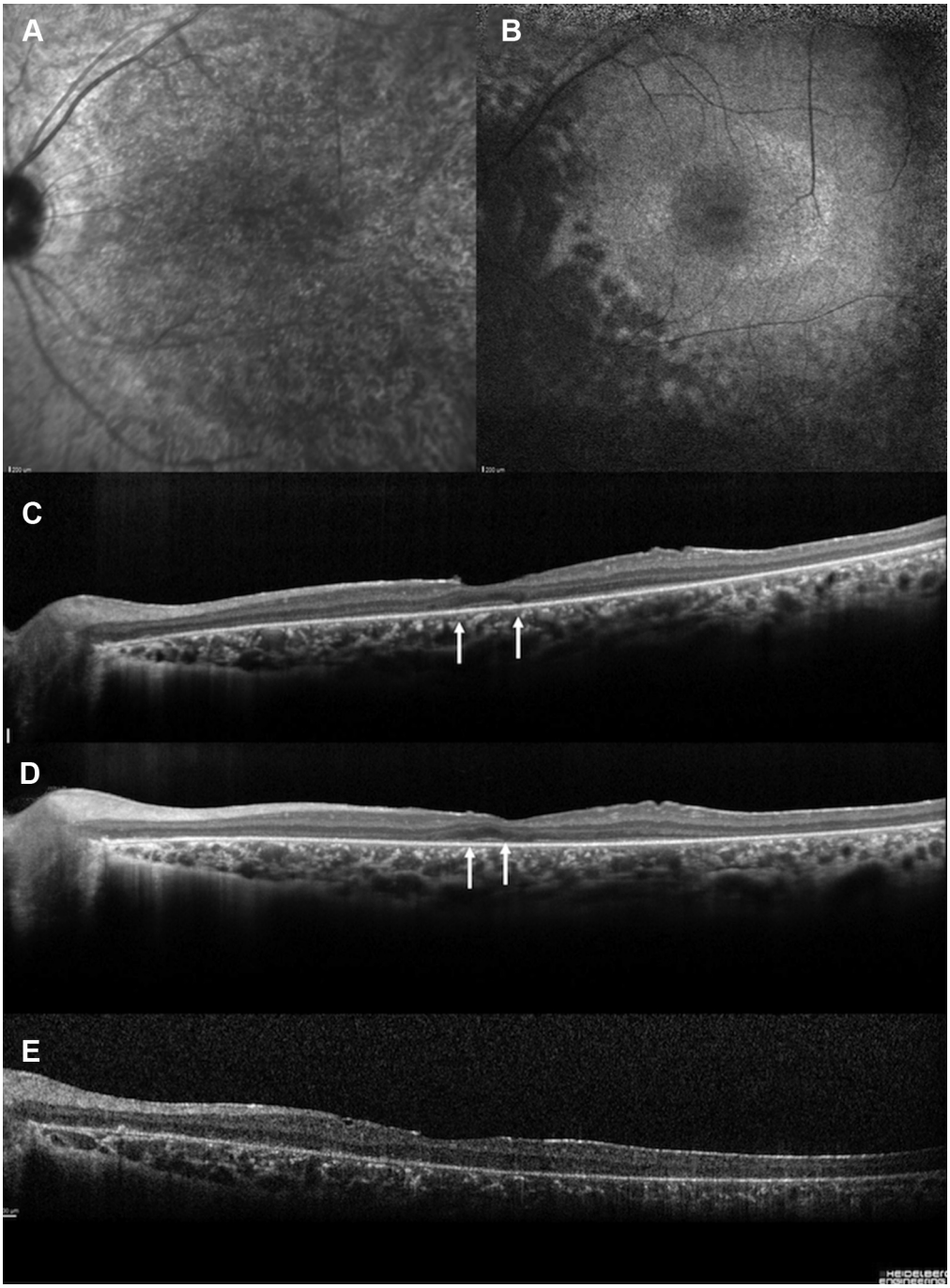

Figure 2. **A**–**E**, Images from a 28-year-old woman (patient RP3186) with the homozygous c.203delA pathogenic variant with a severe form of retinitis punctata albescens in line with a Newfoundland rod–cone dystrophy phenotype. **A**, Infrared reflectance imaging showing a granular and heterogeneous appearance of the entire posterior pole. **B**, Fundus autofluorescence imaging showing that the fovea is oval and hypoautofluorescent. Note a perifoveal annular ring and multiple hypoautofluorescent lesions along the arcades and in the mid periphery. **C**–**E**, Spectral-domain OCT horizontal scans showing the disappearance of the ellipsoid zone (arrows), interdigitation zone (IZ), and outer nuclear layer with time at (**C**) 28 years of age, (**D**) 29 years of age, and (**E**) 31 years of age.

predicted to be pathogenic by Polyphen-2, Mutation taster, Provean, and Mobidetails software. This variant is present in gnomAD at a very low frequency (minor allelic frequency, 6.138e-5), compatible with the recessive mode of inheritance of the disease, and was never found in the homozygous state.

Functional Clinical Assessment

The clinical findings are summarized in Tables 1 and 2. The cohort comprised 11 female and 10 male participants with a mean age of 26.4 years (21 patients; age range, 3–57 years)

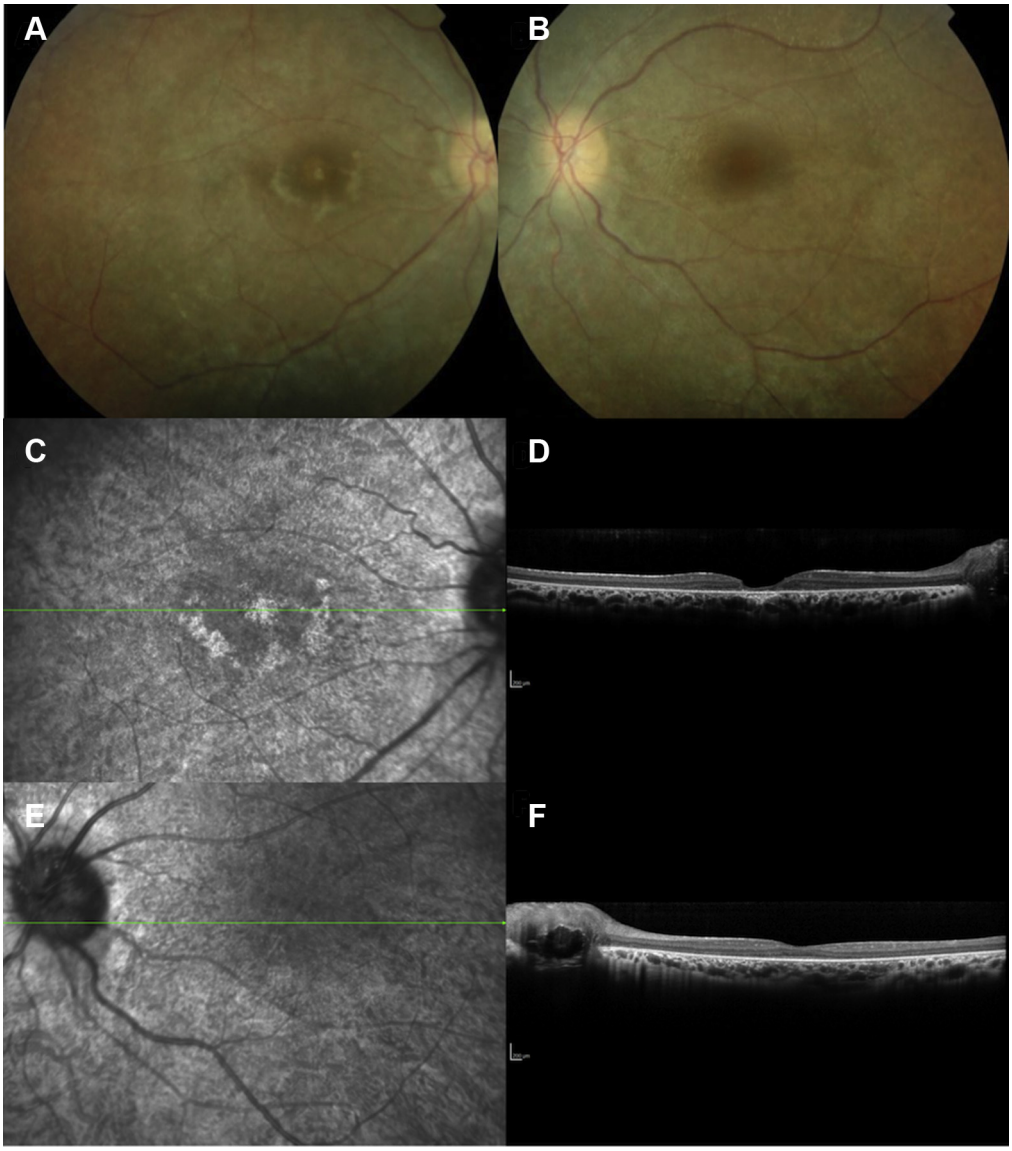

Figure 3. A–F, Images from a 23-year-old woman with retinitis pigmentosa demonstrating white dots and an early macular involvement in line with a Bothnia dystrophy phenotype as well as optic nerve head drusen in both eyes. Night blindness was noted at the age of 2 years. Visual acuity was 20/200 in the right eye and 20/40 in the left eye. At the age of 28 years, visual acuity was less than 20/200 in both eyes. **A–D**, In the (**A**, **B**) color photographs and (**C**, **D**) infrared reflectance photographs, the retina is whitish and the main retinal vessel diameters are reduced. In the right eye, foveal and perifoveal atrophy is noted. **E**, **F**, Spectral-domain OCT horizontal macular scans of the (**E**) right eye and (**F**) left eye: the ellipsoid zone (EZ) and interdigitation zone (IZ) are not visible and the foveal thickness is severely reduced in the right eye, whereas in the left eye, the foveal thickness is decreased without outer nuclear layer and EZ and IZ sharp detection.

at the first visit and 32.4 years (19 patients; range, 11–62 years) at last visit. Independently of the RPA subtype, night blindness was a common feature perceived in early childhood. One patient (patient RP2632-1) reported night blindness and moderate visual decline only after 40 years of age. Visual acuity was asymmetrical in 11 patients. However, over the entire cohort, the right and left eyes were comparable, and no statistical difference was observed. Visual acuity distribution over the entire the cohort and progression in individual patients with follow-up are also represented graphically in Figures 6 and 7.

In the predominant NFRCD group (17 patients; 34 eyes; age range, 3–57 years; mean age, 25.9 years), mean initial and final visual acuity were 0.53 ± 0.50 in logarithm of the minimum angle of resolution (Snellen equivalent, 20/50) and 0.52 ± 0.45 logarithm of the minimum angle of resolution (Snellen equivalent, 20/60), respectively. Severity varied between members of the same family and between different families. Visual acuities of the 5 patients with NFRCD seen in the third decade varied from counting fingers (patient RP1838-3) to 20/25 (patient RP1633-3). In family RP2610, one brother had a visual acuity of 20/25 in

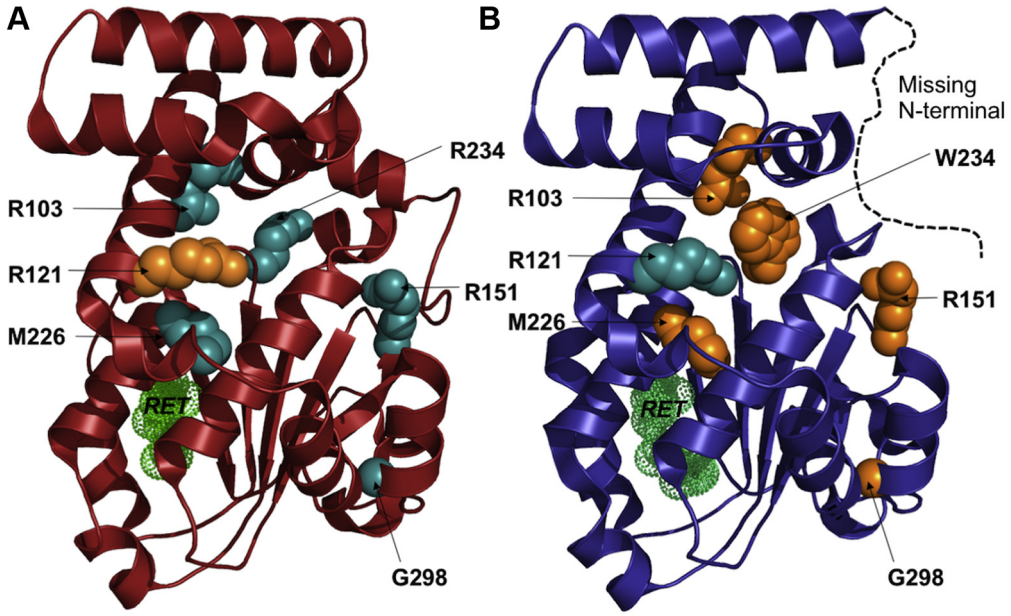

Figure 4. **A**, **B**, Diagrams showing cellular retinaldehyde-binding protein (CRALBP) mutations and structures. The 2 known crystal structures of CRALBP are shown with the position of the mutated residues (discussed in the text) displayed as spheres. The retinol is shown in green dots. The wild-type and p.Arg234Trp (patient R234W) structures are drawn in (**A**) red and (**B**) blue ribbons, respectively. The missing N-terminal segment in the p.Arg234Trp (R234W) structure is drawn as a black dashed line. The mutation favoring the wild-type p.Arg121Trp (R121W) or the rearranged (p.Arg103Trp [R103W], p.Arg151 Gln/Trp [R151Q/W], p.Met226Lys [M226K], p.Arg234Trp [R234W], and p.Gly298Asp [G298D]) conformations are shown in cyan and orange spheres, respectively.

the right eye and 20/50 in the left eye at 40 years of age and the other had visual acuities of 20/125 in both eyes at 44 years of age. Similarly, for the BD family (family RP857), 1 of the 2 sisters was legally blind at the age of 35 years, whereas the other showed a visual acuity of 20/50 in the right eye and 20/30 in the left eye when she was 42 years of age. Finally, for the RPA group, visual prognosis was better even in late adulthood.

Fifteen patients had GVF findings available at initial and final examinations (Table 1). According to World Health Organization criteria, initial GVF was preserved in 1 patient, mildly impaired GVF (central visual field between 20° and 70°) was observed in 9 patients, low-vision GVF was observed in 3 patients, and blindness GVF was observed in 2 patients. During follow-up, all patients reported progression of peripheral visual field loss, and the 2 sisters with BD progressed from both mild GVF to low GVF or to blindness GVF.

Multimodal Imaging Assessments

The characteristic white dot-like deposits at the level of the outer retina were observed in all patients on fundus examination by fundus autofluorescence or SD-OCT scan. Fundus autofluorescence frames showed multiple hypoautofluorescent spots overlapping only partially with the white dots. Peripheral retinal pigmentary changes were rare, with progressive occurrence of scallop-shaped peripheral atrophic lesions in advanced disease stages. This is often noted in IRDs when an atrophy of the RPE occurs before photoreceptor degeneration. The classic perifoveal ring of retinitis pigmentosa was not a common feature in *RLBP1*-associated RCD, detected in only 4 patients (patients RP517-1, RP1633-2, RP3186-1, and RP2610-1).

Macular Thickness and Ellipsoid Zone Width According to Phenotype

All affected patients showed significantly reduced foveal, nasal, and temporal thicknesses, regardless of age, in comparison with control participants (Table 2). Even if most patients belonged to the NFRCD phenotype, the lower values were noted in patients with BD (mean foveal thickness, 109 μm) and the higher values were noted in patients with classic RPA (mean foveal thickness, 205 μm; Table 2). The other retinal measurements also were lower in the BD group versus the NFRCD group and were highest in the classic RPA group. The ellipsoid zone (EZ) width of each individual is represented in Figure 6. Over time, the fovea thinned and the EZ width decreased in the BD and NFRCD groups (Fig 7). No progression was detectable in the 2 patients with RPA, with a follow-up of 69 and 118 months.

Macular Thickness and Ellipsoid Zone Width as a Function of Visual Acuity

Correlations between visual acuities and retinal thicknesses also were analyzed independent of the clinical phenotypes to define SD OCT prognostic values. The data are summarized in Table 2 and shown in Figures 6 and 7. A parallel could be seen

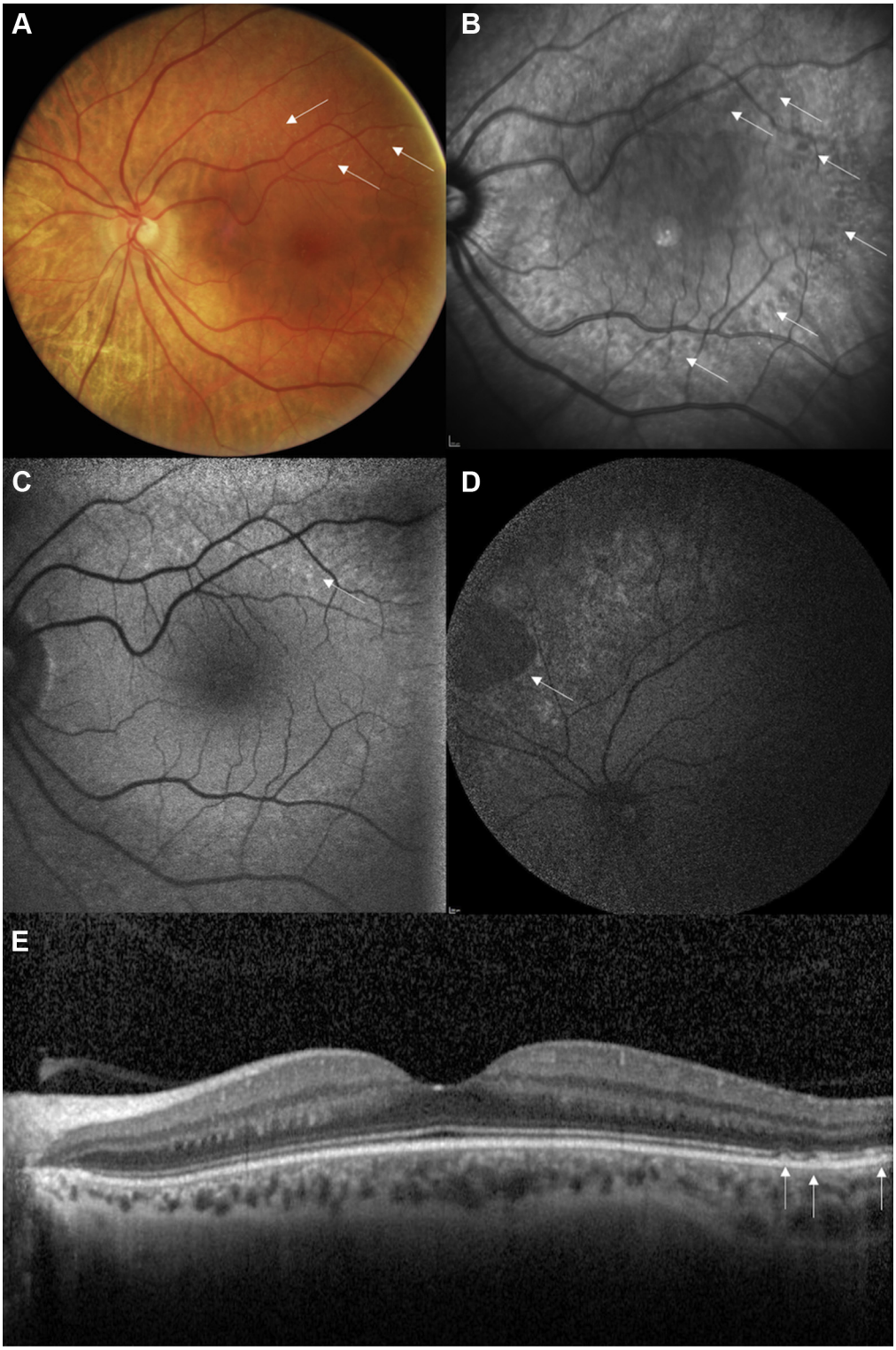

Figure 5. A—E, Images showing unusual late-onset retinitis punctata albescens in a 51-year-old woman with a very mild form of the disease, noting night blindness only since the age of 40 years. Visual acuity was 20/20 in both eyes. **A**, **B**, Note the (**A**) white dots (white arrows) on the color photograph and (**B**) more numerous dark round lesions (white arrows) on the infrared reflectance photograph. **C**, **D**, Autofluorescence imaging showing that the fovea is preserved, whereas (**C**) small hyperautofluorescent dots (arrows) appear along the superior temporal arcades and (**D**) scallop-bordered atrophic lesions appear in the mid-peripheral retina (arrows). **E**, Spectral-domain OCT horizontal scan showing that the macular segmentation is preserved with typical white dots lesions in the temporal retina (white arrows).

Table 1. Clinical and Genetic Data of the 21 Patients with Biallelic Pathogenic Variants in *RLBP1*

Patient Identifier	Age at Initial Visual Acuity and Visual Field Assessment	Gender	Night Blindness	Initial Visual Acuity (Right Eye, Left Eye)			Final Visual Acuity (Right Eye, Left Eye)			Visual Field (Right Eye, Left Eye)*				Follow-up (mos)	Reading Difficulties	Pathogenic Variations
				Snellen	*Logarithm of the Minimum Angle of Resolution*	*Age (yrs)*	*Snellen*	*Logarithm of the Minimum Angle of Resolution*	*Age (yrs)*	*Initial*	*Age (yrs)*	*Final*	*Age (yrs)*			
NFRCD phenotype (17 patients, 12 families)																
RP1554-1	3	F	3	20/20, 20/20	0, 0	3	20/20, 20/20	0, 0	13	Normal	10	Normal	13	123	N	Exons 7_9del/Exons 7_9del Exons 7_9del/Exons 7_9del
RP1789-1	3	M	2	20/25, 20/25	0.1, 0.1	3	20/25, 20/25	0.1, 0.1	11	ND		Normal	11	92	N	Exons 7_9del/Exons 7_9del Exons 7_9del/Exons 7_9del
PB70	4	F	4	20/40, 20/50	0.3, 0.4	4	20/125, 20/125	0.8, 0.8	16	ND		Low		156	Y	c.753C>A, p.Tyr251* (ex 8) c.753C>A, p.Tyr251* (ex 8)
RP3451-1	10	F	4	20/32, 20/32	0.2, 0.2	10	20/32, 20/63	0.2, 0.5	13	Mild		Mild		42	N	Exons 7_9del/Exons 7_9del Exons 7_9del/Exons 7_9del
RP3066-1	13	F	5	20/63, 20/63	0.5, 0.5	13	20/63, 20/200	0.5, 1	16	Mild		Mild		36	N	Exons 7_9del/Exons 7_9del Exons 7_9del/Exons 7_9del
RP702-1	24	M	6	20/200, 20/600	1, 1.5	24	20/600, 20/600	1.5, 1.5	31	Low		Low		75	Y, second decade	Exons 7_9del/Exons 7_9del Exons 7_9del/Exons 7_9del
RP517-1	32	M	3	20/30, 20/40	0.2, 0.3	32	20/125, 20/100	0.8, 1	50	Low		Low		210	N	Exons 7_9del/Exons 7_9del Exons 7_9del/Exons 7_9del
RP1633-3	29	F	4	20/30, 20/25	0.2, 0.1	29	20/30, 20/25	0.2, 0.1	31	Mild		Mild		19	N	Exons 7_9del/Exons 7_9del Exons 7_9del/Exons 7_9del
RP 1633-2	32	M	4	20/63, 20/63	0.5, 0.5	32	20/63, 20/100	0.5, 1	33	Mild		Mild		19	N	Exons 7_9del/Exons 7_9del Exons 7_9del/Exons 7_9del
RP1633-1	39	F	4	20/25, 20/20	0.1, 0	39	20/25, 20/25	0.1, 0.1	40	Mild		Mild		19	N	Exons 7_9del/Exons 7_9del Exons 7_9del/Exons 7_9del
RP1838-1	22	F	2	20/32, 20/32	0.2, 0.2	22	NFU	NFU	NFU	Mild		NFU		0	N	Exons 7_9del/Exons 7_9del Exons 7_9del/Exons 7_9del
RP1838-3	26	M	5	20/800, 20/800	1.6, 1.6		NFU	NFU	NFU	Low		NFU		0	Y, 23 yrs	Exons 7_9del/Exons 7_9del Exons 7_9del/Exons 7_9del
RP1838-2	34	M	3	20/400, 20/400	1.3, 1.3	34	HM, LP		42	Low		ND		100	Y, 27 yrs	Exons 7_9del/Exons 7_9del Exons 7_9del/Exons 7_9del
RP3186-1	28	F	2	20/200, 20/400	1, 1.3	28	HM, HM		31	Blindness		Blindness		38	Y, second decade	c.203delA, p.Glu68Glyfs*51 (exon 5) c.203delA, p.Glu68Glyfs*51 (exon 5)
RP2610-1	40	M	3	20/25, 20/50	0.1, 0.4	40	20/32, 20/63	0.2, 0.5	46	Low		Low		75	N	c.46C>T, p.Gln16* (exon 4) c.466C>T, ≥ p.Arg156* (exon 6)
RP2610-2	44	M	5	20/125, 20/125	0.8, 0.8	44	NFU	NFU	NFU	Low		NFU		NFU	Y, 35 yrs	c.46C>T, p.Gln16* (exon 4) c.466C>T, p.Arg156* (exon 6)
RP1682-1	57	M	6	20/50, 20/50	0.4, 0.4	57	20/63, 20/63	0.5, 0.5	62	Blindness		Blindness		54	Y, 55 yrs	c.488insA, p.Ileu163Asnfs*1 (exon 6) c.488insA, p.Ileu163Asnfs*1 (exon 6)
BD phenotype (2 related patients)																
RP857-1	23	F	2	20/125, 20/40	0.8, 0.3	23	20/400, CF	1.3, CF	35	Mild + central scotoma		Blindness		144	Y, in childhood	c.333T>G, p.Tyr111* (exon 5) c.700C>T, p.Arg234Trp (exon 8)
RP857-2	28	F	3	20/32, 20/25	0.2, 0.1	28	20/50, 20/32	0.4, 0.2	42	Mild		Low		167	N	c.333T>G, p.Tyr111* (exon 5) c.700C>T, p.Arg234Trp (exon 8)

Table 1. (Continued.)

Patient Identifier	Age at Initial Visual Acuity and Visual Field Assessment	Gender	Night Blindness	Initial Visual Acuity (Right Eye, Left Eye)			Final Visual Acuity (Right Eye, Left Eye)		Visual Field (Right Eye, Left Eye)*			Follow-up (mos)	Reading Difficulties	Pathogenic Variations
				Snellen	Logarithm of the Minimum Angle of Resolution	Age (yrs)	Snellen	Logarithm of the Minimum Angle of Resolution	Age (yrs)	Initial	Final	Age (yrs)			
RPA phenotype (2 unrelated patients)														
RP1254-1	13	M	4	20/16, 20/20	−0.1, 0	13	20/20, 20/20	0, 0	23	Mild	Mild		118	N	c.25C>T, p.Arg9Cys (exon 4) c.333T>G, p.Tyr111* (exon 5)
RP2632-1	51	F	40	20/20, 20/20	0, 0	51	20/30, 20/40	0.2, 0.5	57	Mild	Mild		69	N	c.361C>T, p.Arg121Trp (exon 6) c.677T>A, p.Met226Lys (exon 7)

BD = Bothnia dystrophy; CF = counting fingers; F = female; HM = hand movements; LP = light perception; M = male; N = no; ND = not done; NFRCD = Newfoundland rod–cone dystrophy; NFU = no follow-up; RPA = retinitis punctata albescens; Y = yes.
*Classified based on the criteria of the World Health Organization (mild visual impairment for a central visual field between 20° and 70°, low vision if limited to the central 20°, and blindness if inferior to 10°).

between visual acuity and retinal thinning in all locations and between visual acuity and EZ line width: the lower the visual acuity, the thinner the retina and the shorter the EZ. Overall, in the group of patients with a visual acuity of better than 20/200, none demonstrated a foveal thickness of less than 130 μm, and all but 1 patient (patient RP1682) demonstrated an EZ width of more than 1200 μm (Fig 8).

Discussion

In the current gene therapy context, we reappraised a large cohort of patients with *RLBP1* pathogenic variants seen in a single national reference center to correctly establish the correlations between all biallelic combinations of pathogenic variants and their associated phenotypes. Overall, the classic RPA phenotype is rare (2/21 patients) in southern France, whereas severe phenotypes are frequent, with a high incidence of NFRCD (17/21 patients). These severe phenotypes being associated with a worse prognosis justify an early indication of gene therapy before visual acuity drops to worse than 20/200. Because of intrafamilial and interfamilial variations, morphologic criteria based on outer retinal layer assessment with SD-OCT should be considered, that is an ellipsoid width of more than 1200 μm and a foveal thickness of more than 130 μm.

Novel Pathogenic Variants

We also reported 3 novel pathogenic *RLBP1* variants. First, the p.Gln16* variant located in exon 4 probably activates NMD. Nonsense-mediated mRNA decay is an evolutionarily conserved and critical cellular surveillance mechanism that recognizes and eliminates aberrant mRNAs containing premature termination codons (located at least 50–55 nucleotides upstream of the last exon–exon junction) or abnormally long untranslated regions.[28] Nonsense-mediated mRNA decay was found to affect one-third of the mutated mRNAs.[29] Second, the nonsense p.Tyr251* variant located in exon 8 is predicted to lead to a truncated protein and therefore disrupting the CRAL-TRIO lipid-binding domain (162 amino acids from position 136 to 297). However, because of the position of this variant in the penultimate exon, it alternatively could undergo NMD, which would lead to absence of protein production. Finally, the p.Arg121Trp variant, situated near the p.Gly116Arg variant described by Naz et al,[11] is predicted to be damaging by PolyPhen-2 software and to affect protein function according to the Provean, Mobidetails, and Mutation taster databases. The frequency of this variant in the gnomAD exome database (0.0000478) is compatible with an autosomal recessive transmission. Moreover, the Grantham score (value = 101) for this amino acid change is high, with a good conservation at this position across species (Genomic Evolutionary Rate Profiling score, 4.65). This variant of uncertain significance is reappraised as likely pathogenic when in *trans*with a pathogenic variant according to ACMG pathogenicity criteria. Taken together, these 3 novel *RLBP1* variants raise the total number reported to 45 variants (Fig 9).

Table 2. Visual Acuity and Spectral-Domain OCT Measurements for Each Phenotype and Control Participant

	Bothnia Dystrophy (n = 4 Eyes)	Newfoundland Rod–Cone Dystrophy (n = 34 Eyes)	Retinitis Punctata Albescens (n = 4 Eyes)	Control Participants (n = 28 Eyes)	*P* Value*	*P* Value†
Visual acuity (logMAR)						
Initial	0.35 ± 0.31	0.53 ± 0.50	−0.03 ± 0.05	—	—	0.27
Final	0.63 ± 0.59	0.52 ± 0.45	0.18 ± 0.24	—	—	0.43
Foveal thickness						
Initial	109.25 ± 42.91	167.50 ± 38.22	204.75 ± 3.30	226.79 ± 20.71	<0.01	0.05‡
Final	94.25 ± 40.06	148.22 ± 49.15	204.75 ± 2.75	—	—	0.13§
EZ width						
Initial	3096 ± 2552	6229 ± 2771	7306 ± 353	—	—	0.16
Final	2944 ± 2481	6331 ± 2675	7276 ± 360	—	—	0.24
Nasal						
At 1500						
Initial	243.50 ± 13.38	268.77 ± 22.19	316.50 ± 49.57	347.21 ± 19.29	<0.01	0.04‡
Final	240.50 ± 15.33	258.83 ± 20.63	312.75 ± 42.52	—	—	0.05‡
At 3000 μm						
Initial	307.00 ± 42.61	243.14 ± 30.05	265.50 ± 29.49	293.32 ± 24.27	<0.01	0.03‖
Final	266.25 ± 20.47	233.94 ± 28.71	248.00 ± 36.15	—	—	0.28
Temporal						
At 1500 μm						
Initial	209.25 ± 19.87	241.64 ± 33.92	308.00 ± 46.05	321.46 ± 19.03	<0.01	0.03¶
Final	209.75 ± 12.66	229.78 ± 28.04	303.00 ± 43.95	—	—	0.02¶
At 3000 μm						
Initial	183.75 ± 16.56	212.41 ± 39.32	236.25 ± 28.63	257.89 ± 17.08	<0.01	0.34
Final	181.75 ± 16.36	205.78 ± 35.99	231.25 ± 27.54	—	—	0.33

EZ = ellipsoid zone; logMAR = logarithm of the minimum angle of resolution; − = not apllicable.
Values represented as mean±standard deviation, unless otherwise indicated.
*Comparisons between control participants and the 3 pooled phenotypes using a linear mixed model adjusted for age with participant as the random effect.
†Comparisons among the 3 phenotypes using a linear mixed model adjusted for age with participant as the random effect. Tukey's correction was applied for pairwise comparisons.
‡Retinitis punctata albescens > Newfoundland rod–cone dystrophy.
§Bothnia dystrophy < retinitis punctata albescens.
‖Newfoundland rod–cone dystrophy < Bothnia dystrophy.
¶Retinitis punctata albescens > Bothnia dystrophy and Newfoundland rod–cone dystrophy.

Protein-Truncating Variants Are Associated with Newfoundland Rod–Cone Dystrophy

To date, NFRCD has been associated with *RLBP1* splice variants. This severe phenotype was well documented in several publications, and 3 variants (c.142-1G>A, c.141G>A, and c.141+2T>C) affecting exon 4 or 5 splicing were described.[3,15] None of our patients carried these biallelic splice variants. By contrast, other protein-truncating variants were found in our cohort. All the Moroccan patients carried the previously described 7.36-kb deletion of the 3 last *RLBP1* exons, suggesting that these patients inherited the mutant allele from a common ancestor.[23] All the other patients showed a combination of nonsense variants and small insertions and deletions and a severe phenotype in line with a NFRCD, but with notable intrafamilial variation. It is likely that these variants were targeted by NMD. Nonsense-mediated mRNA decay is a potent modulator of disease severity and clinical phenotype in light of its important role in recognizing and degrading mutated transcripts. It has been suggested that NMD would worsen the severity of the disease. Furthermore, full or partial NMD has been shown previously for variants in IRD genes such as *EYS* and thus could explain the severity variation noted between and within families.[30]

In addition, Hipp et al[14] described a novel splice variant, c.684+1del, affecting exon 7 that one could expect to be associated with a severe phenotype in patients with typical and moderate RPA phenotype (preserved visual acuity at 60 and 68 years of age). This discrepancy could be explained by the loss of the consensus donor site and the use of a cryptic site, one base pair upstream according to Mobidetails predictions and leading to a frameshift and the creation of a stop codon in exon 8. A truncated protein thus could be produced because the NMD pathway would be ineffective as a result of the presence of the novel stop codon so far into the penultimate exon of the gene. Thus, splice variations should be analyzed individually because they either can act as null alleles (for example, p.Tyr251*) or can lead to alternative proteins (for example, c.684+1del).

New Allelic Combination Leading to Bothnia Dystrophy

Bothnia dystrophy is characterized by early macular involvement and severe visual loss resulting from a toxic effect of the mutant protein. The Bothnian variants induce a rearrangement of the ligand-binding cavity, leading to an increased binding to 11-cis-retinal and a reduced rate of

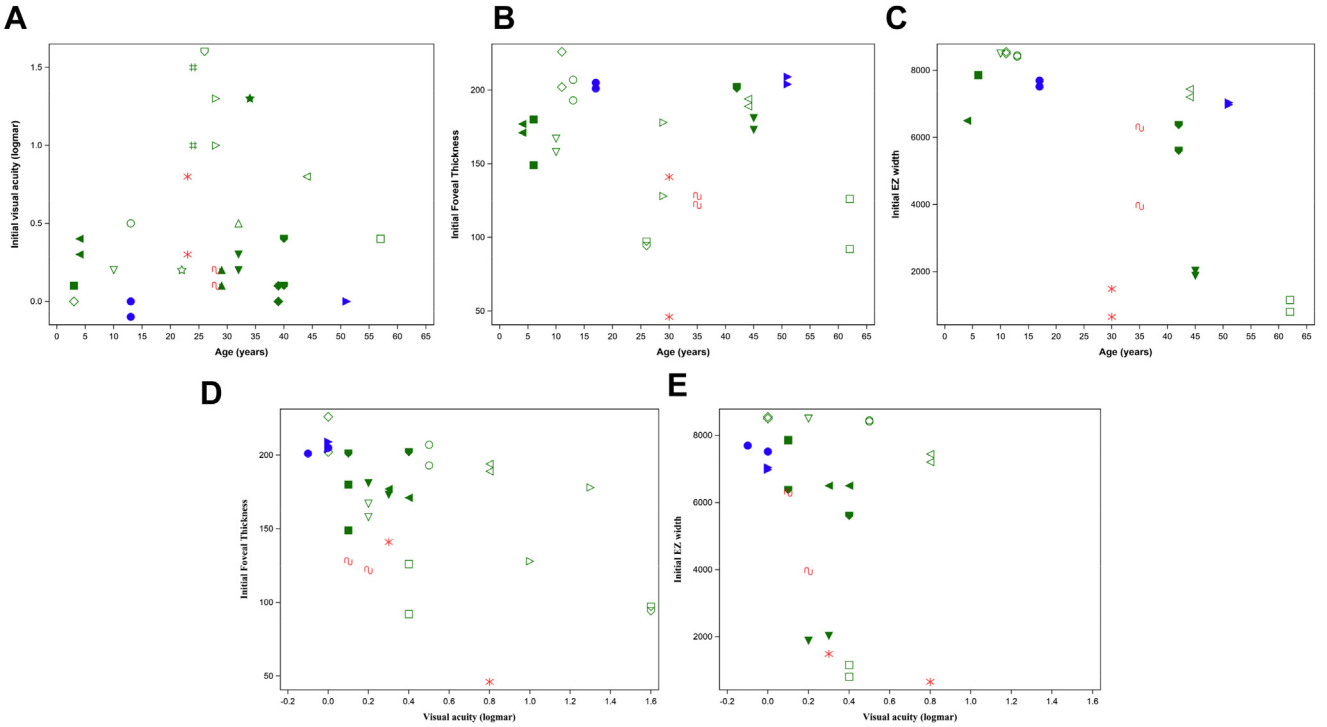

Figure 6. **A**–**E**, Graphs showing initial clinical data of 12 patients with Newfoundland rod–cone dystrophy in green, 2 patients with Bothnia dystrophy in red, and 2 patients with retinitis punctata albescens in blue. A different symbol appears for each participant (the same per eye): (**A**) visual acuity, (**B**) foveal thickness, (**C**) ellipsoid zone (EZ) width according to age, (**D**) foveal thickness, and (**E**) EZ width according to visual acuity.

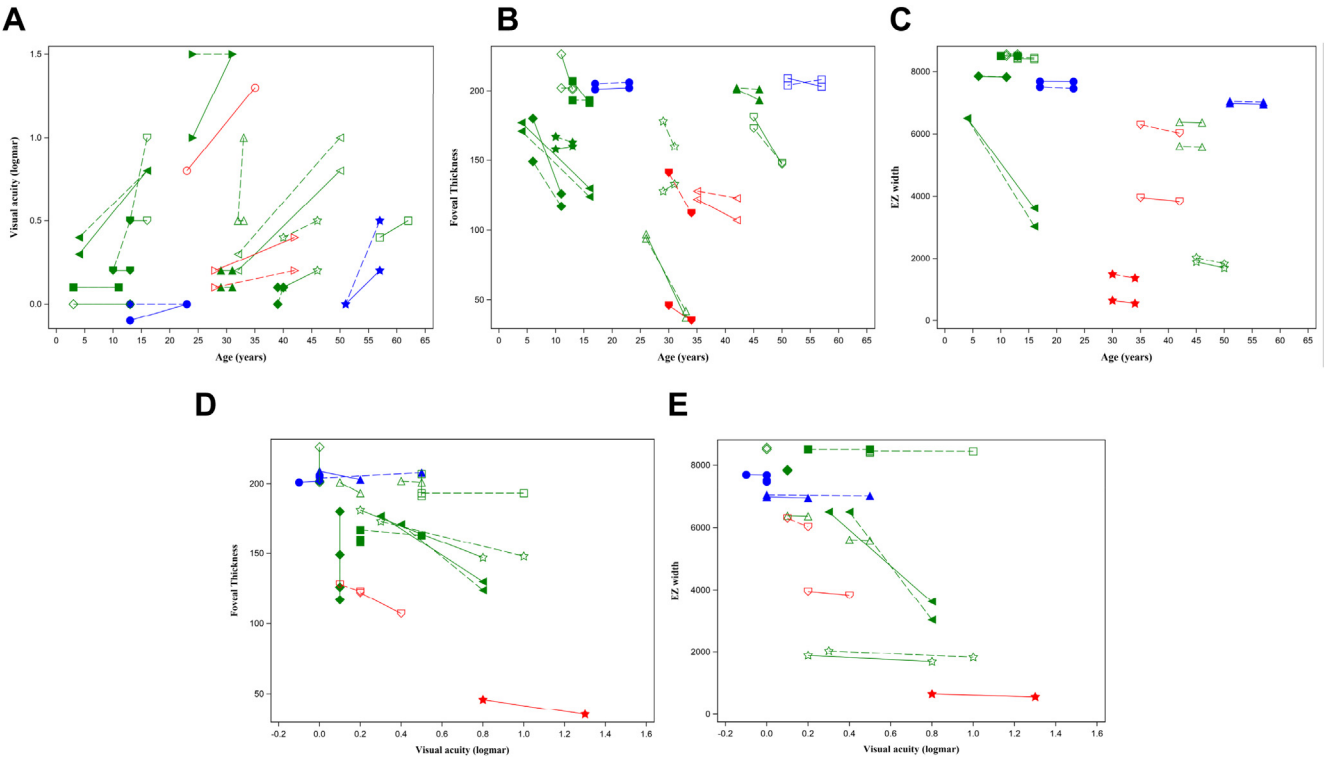

Figure 7. **A**–**E**, Graphs showing follow-up clinical data analyses of 12 patients with Newfoundland rod–cone dystrophy in green, 2 patients with Bothnia dystrophy in red, and 2 patients with retinitis punctata albescens in blue. The evolution of the right eye is represented by a dotted line and that of the left eye by a solid line. A different symbol appears for each participant: evolution over time of (**A**) visual acuity, (**B**) foveal thickness, (**C**) ellipsoid zone (EZ) width according to age, (**D**) foveal thickness, and (E) EZ width according to visual acuity.

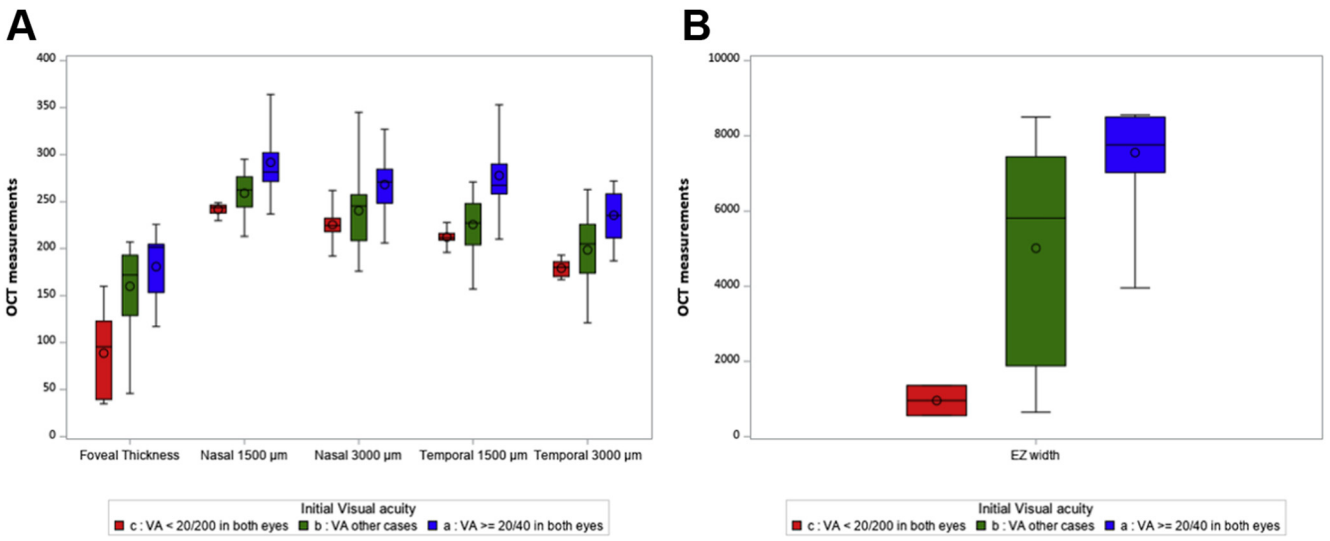

Figure 8. **A**, **B**, Box-and-whisker plots showing representation of the distributions of all OCT measurements for all participants according to their level of visual acuity (VA) at the time of measurement: red represents VA of worse than 20/200 in both eyes, blue represents VA of 20/40 or better in both eyes, and green represents other cases. EZ = ellipsoid zone.

ligand photoisomerization. To date, reported patients with BD are either homozygous or compound heterozygotes for p.Met226Lys and p.Arg234Trp. Based on family RP857, we demonstrate that a BD phenotype also can arise when one of the Bothnia variants is in *trans* with a null allele (deletion, nonsense, or splicing variants).

Reappraisal of Pathogenic Variants Leading to Retinitis Punctata Albescens

A milder RPA phenotype can be encountered in all combinations of biallelic missense variants, even compound heterozygotes for a BD variant. For example, patient RP2632 carrying the BD variant p.Met226Lys in *trans* with the p.Arg121Trp variant did not demonstrate BD.

We tried to elucidate the effect of the missense variants described herein or in the literature further by reappraising their impacts on the crystal structures of CRALBP.[27] To date, only the precise molecular mechanism of p.Arg234Trp has been studied.[31] A significant and local rearrangement occurs on substitution of the arginine at position 234 by a tryptophan. In the 2 crystal structures, the wild-type and the mutant p.Arg234Trp and the 229 to 236 amino acids loop adopt a different conformation, and the 27 to 56 amino acids N-terminal segment is visible only in the wild-type structure, although the mutant was refined

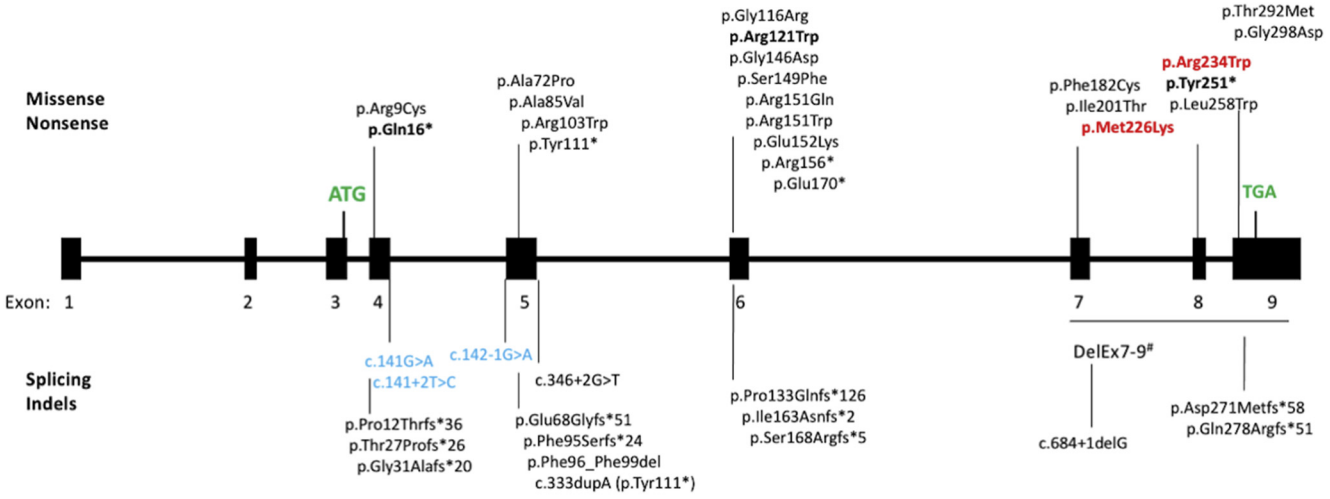

Figure 9. Diagram showing the spectrum of *RLBP1* pathogenic variations (at the protein or cDNA level) reported in *RLBP1*. Boldface data represent novel variants described herein. The top half identifies missense and nonsense variants, whereas the bottom half identifies splice and insertion and deletion variants. Variants previously described in Bothnia dystrophy appear in red. Variants previously described in Newfoundland rod–cone dystrophy appear in blue. Start (ATG) and stop (TGA) codons appear in green. Exons 3 to 9 are coding exons. Five entries are listed in HGMD Pro for this large deletion.

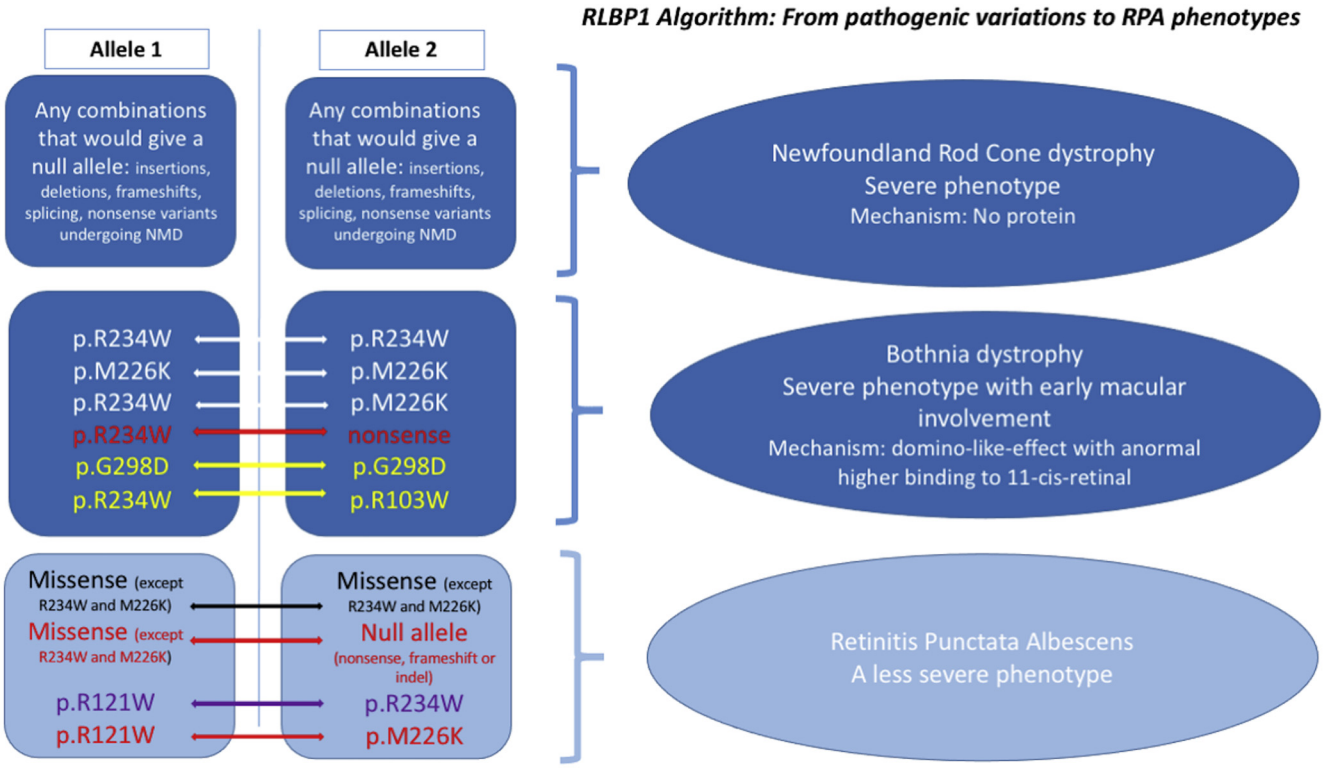

Figure 10. A proposed algorithm from variant combinations to phenotypes. On the left are a combination of alleles (1 and 2). Data from the present work appear in red. Reappraisal of data from the literature appear in yellow. A combination including 1 Bothnia dystrophy variant, but leading to classic retinitis punctata albescens (RPA), appears in purple. On the right is an associated phenotype. NMD = nonsense-mediated mRNA decay.

at a much higher resolution (1.7 Å vs. 3.0 Å). Accordingly, we modeled each mutant in the 2 experimental conformations in an attempt to evaluate putative shift in the conformation equilibrium, and hence their potential phenotypic impact.

First, 2 variants—p.Arg103Trp and p.Arg121Trp (family RP2632)—occur at the surface of the protein, whereas 3 others—p.Met226Lys, p.Arg151Gln or p.Arg151Trp, and p.Gly298Asp—may be more detrimental because they occur at buried positions.[4,10,13,14] The Met226 residue is buried fully, and its substitution to a positively charged lysine would imply strong destabilization of the wild-type conformation. However, the lysine would be able to interact favorably with the Ser230 sidechain in the p.Arg234Trp conformation. Hence, the variant p.Met226Lys could favor a conformation similar to that observed for p.Arg234Trp, and hence could account for the BD phenotype.

For the variant p.Gly298Asp, the numerous close contacts with neighboring residues (Glu141 and Gly143) suggest that the protein cannot accommodate the change toward a larger and negatively charged residue, such as aspartate. Accordingly, this mutation is predicted to destabilize the protein at least locally. Of note, the N-terminus extension in the wild-type conformation brings the Phe34 in close contact with the short α-helix 298−306. Hence, destabilization of this helix by the mutation could promote unfolding of the N-terminal segment, as observed in the p.Arg234Trp mutant structure. Again, such a mutation could mimic the impact of p.Arg234Trp or p.Met226Lys while lying in a distinct portion of the protein.

For the variant p.Arg103Trp, modeling on the low-resolution wild-type structure suggests that the substitution would destabilize the conformation partially because of the loss of a salt bridge with Asp229 (distance: Arg103-NH2−Asp229-OD1). Interestingly, in the high-resolution structure of the variant p.Arg234Trp, this salt bridge is already broken. Furthermore, the side chain of a tryptophan at position 103 could point toward the Leu113 (as in the wild-type structure), but also toward the rearranged Ala233. This additional interaction may impact the conformational equilibrium toward a BD structure like the p.Arg234Trp variant.

Concerning position 151, in the case of the change of the arginine toward a smaller glutamine, hydrogen bonds with the side chains of Asn190 and Thr193 would be lost. The change toward a large tryptophan may add favorable hydrophobic interactions with Va133 and Va1157. Of note, the position 151 is solvent exposed in the high-resolution p.Arg234Trp mutant structure, whereas it is buried in the low-resolution wild-type protein, in which the N-terminus is better resolved. Accordingly, neither of these 2 substitutions at position Arg151 would be too detrimental for the folding of the protein. Nevertheless, neither the glutamine nor the

tryptophan side chain can perfectly mimic the arginine. In this case, a definitive conclusion is more difficult to draw.

Finally, the p.Arg121Trp variant would stand apart. Arg121 is partially buried because it is sandwiched between 2 aromatic and hydrophobic residues, Tyr117 and Phe128, in both the wild-type and the mutant p.Arg234Trp structures. Mutation toward a large, hydrophobic, and aromatic sidechain would be rather favorable. However, in the wild-type structure, the arginine side chain is pointing toward the Glu185 to form a salt bridge and toward the Tyr117 to form a weak hydrogen bond, whereas in the variant structure, it is hydrogen bonded to Ser230 and also to Glu185 (but through a water molecule). All these interactions would be lost in the mutant p.Arg121Trp. More importantly, the p.Arg121Trp may prevent the rearrangement because of unfavorable interactions with the serine Ser230. As such, the p.Arg121Trp may have a so-called reverse BD effect by favoring the wild-type conformation.

Accordingly, and taking into account the distinct resolution of the crystal structures of the wild-type and p.Arg234Trp variant as a marker of intrinsic flexibility, one could imagine a scenario whereby the wild-type protein is rather flexible, although folded and functional, whereas some disease-related variants are frozen in a conformation similar to that observed for the p.Arg234Trp variant. Hypothetically, this would decrease the release of the ligand; however, this remains to be confirmed. To summarize, we have reappraised the different variant combinations and their related phenotypes in Figure 10.

Importance of Spectral-Domain OCT-Relevant Criteria

Spectral-domain OCT or fundus autofluorescence imaging can provide additional specific criteria as indications for gene therapy. The perifoveal ring delineating the central preserved retina is not relevant in *RLBP1*-related retinal dystrophy because of its low frequency (4/21 patients). However, foveal, temporal, or nasal thinning are observed at early stages, even in young patients and in the absence of central visual loss. For example, in eyes with a visual acuity of more than 20/40, the mean foveal thickness is 186 μm (standard deviation, 25 μm). This finding is in line with the previous report of early cone degeneration in RPA. An M-cone degeneration was described in *rlbp1*$^{-/-}$ mice with a mislocalization of M-opsin to the cone cell bodies instead of the cone outer segment.[5] Cone degeneration also is linked to a specific role of Müller cells in the cone visual cycle. Furthermore, the nasal and temporal thinning progressed more rapidly in the temporal zone at 1500 μm. In patients with BD, the mean foveal thickness was 109 μm, similar to the value found in eyes with NFRCD and visual acuity worse than 20/200.

Based on SD-OCT data correlated with visual acuity levels, a foveal thickness of more than 130 μm with persistent external limiting membrane and interdigitation zone (IZ) is probably required to maintain a visual acuity of better than 20/200. By comparison, a foveal thickness of more than 100 μm was retained as the indication for *RPE65* gene therapy. Similarly, and even if a large range in EZ width (from 457 to 8411 μm) exists, this width is correlated clearly with visual acuity levels, as shown in Figure 8. Ellipsoid zone width was less than 750 μm in all eyes with a visual acuity of less than 20/200. Only 1 patient with a visual acuity of better than 20/200 showed an EZ width of less than 1100 μm and a foveal thickness of less than 130 μm.

In conclusion, we showed that NFRCD is associated with nonsense variations, deletions, and certain splicing variants in both alleles. By contrast, BD is associated with specific variants in either both alleles or in 1 allele in *trans* with a null allele. Under these latter conditions, gene therapy should not be delayed, but rather should be planned in the first 2 decades of life, before the occurrence of a severe photoreceptor loss or a macular lesion. Furthermore, regardless of phenotype, an EZ of more than 1100 μm and a central thickness of more than 130 μm on SD-OCT are the additional 2 major anatomic criteria that should be fulfilled for gene therapy eligibility.

Acknowledgments

The authors thank the patients and their families.

Footnotes and Disclosures

Originally received: April 23, 2021.
Final revision: August 4, 2021.
Accepted: August 6, 2021.
Available online: August 17, 2021. Manuscript no. D-21-00073.

[1] National Reference Centre for Inherited Sensory Diseases, Univ. Montpellier, Montpellier University Hospital, Montpellier, France, and Sensgene Care Network, ERN-EYE Network, France.

[2] Institute for Neurosciences of Montpellier (INM), Univ. Montpellier, INSERM, Montpellier, France.

[3] Molecular Genetics Laboratory, Univ. Montpellier, Montpellier University Hospital, Montpellier, France.

[4] Centre for Structural Biology, Univ. Montpellier, INSERM, CNRS, Montpellier, France.

[5] Department of Ophthalmology, University Hospital, Reims, France.

[6] Jules Verne Clinic, Nantes, France, and Sensgene Care Network, France.

[7] Department of Visual Exploration and Neuro-Opthalmology, Robert Salengro Hospital, Lille, France, and Sensgene Care Network, France.

[8] Department of Research and Innovation, Univ. Montpellier, Montpellier University Hospital, Montpellier France.

[9] Department of Ophthalmology, Avignon Hospital Centre, Avignon, France.

[10] Department of Ophthalmology, Rive Gauche Clinic, Toulouse, France.

[11] Clinical Investigation Center, Clinical Research and Epidemiology Unit, Montpellier, France.

[12] Sorbonne University, INSERM, CNRS, Vision Institute, Paris, France CHNO des Quinze-Vingts, INSERM-DGOS CIC 1423, Paris, France and Sensgene Care Network, ERN-EYE Network, France.

[13] Université de Lille, Inserm, Lille University Hospital, U1172-LilNCog-Lille Neuroscience and Cognition, Lille, France.

Disclosure(s):

All authors have completed and submitted the ICMJE disclosures form.

The author(s) have made the following disclosure(s): I.A.: Consultant — Novartis, Sparing Vision

B.B. and I.M. have had full access to all the data and take responsibility for the integrity of the data and the accuracy of their analysis.

HUMAN SUBJECTS: Human subjects were included in this study. All methods were carried out in accordance with approved protocols of the Montpellier University Hospital, and in agreement with the Declaration of Helsinki. The Ministry of Public Health accorded approval for biomedical research under the authorization number 11018S. Signed informed consent for clinical examination and genetic analysis was obtained.

No animal subjects were included in this study.

Author Contributions:

Conception and design: Bocquet, El Alami Trebki, Roux, Labesse, Brabet, Arndt, Zanlonghi, Defoort-Dhellemmes, Hamroun, Boulicot-Séguin, Lequeux, Picot, Huguet, Audo, Dhaenens, Kalatzis, Meunier

Analysis and interpretation: Bocquet, El Alami Trebki, Roux, Labesse, Brabet, Arndt, Zanlonghi, Defoort-Dhellemmes, Hamroun, Boulicot-Séguin, Lequeux, Picot, Huguet, Audo, Dhaenens, Kalatzis, Meunier

Data collection: Bocquet, El Alami Trebki, Roux, Labesse, Brabet, Arndt, Zanlonghi, Defoort-Dhellemmes, Hamroun, Boulicot-Séguin, Lequeux, Picot, Huguet, Audo, Dhaenens, Kalatzis, Meunier

Obtained funding: N/A

Overall responsibility: Bocquet, El Alami Trebki, Roux, Labesse, Brabet, Arndt, Zanlonghi, Defoort-Dhellemmes, Hamroun, Boulicot-Séguin, Lequeux, Picot, Huguet, Audo, Dhaenens, Kalatzis, Meunier

Abbreviations and Acronyms:
BD = Bothnia dystrophy; **CRALBP** = cellular retinaldehyde-binding protein; **EZ** = ellipsoid zone; **GVF** = Goldmann visual field; **IRD** = inherited retinal dystrophy; **IZ** = interdigitation zone; **NFRCD** = Newfoundland rod–cone dystrophy; **NMD** = nonsense-mediated mRNA decay; **RPA** = retinitis punctata albescens; **RPE** = retinal pigment epithelium; **RCD** = rod–cone dystrophy; **SD** = spectral-domain.

Keywords:
Bothnia dystrophy, CRALBP, gene therapy, Newfoundland rod–cone dystrophy, retinitis punctata albescens, *RLBP1*, spectral-domain OCT, variant classification, visual cycle, white dots.

Correspondence:
Isabelle Meunier, MD, PhD, Centre National de Référence Maladies Rares, Affections Sensorielles Génétiques, Hôpital Gui de Chauliac, 80, rue Augustin Fliche, 34295 Montpellier, Cedex 5, France. E-mail: i-meunier@chu-montpellier.fr.

References

1. Scimone C, Donato L, Esposito T, et al. A novel RLBP1 gene geographical area-related mutation present in a young patient with retinitis punctata albescens. *Hum Genomics*. 2017;11:18.
2. Burstedt MS, Sandgren O, Holmgren G, Forsman-Semb K. Bothnia dystrophy caused by mutations in the cellular retinaldehyde-binding protein gene (RLBP1) on chromosome 15q26. *Invest Ophthalmol Vis Sci*. 1999;40:995–1000.
3. Eichers ER, Green JS, Stockton DW, et al. Newfoundland rod-cone dystrophy, an early-onset retinal dystrophy, is caused by splice-junction mutations in RLBP1. *Am J Hum Genet*. 2002;70:955–964.
4. Maw MA, Kennedy B, Knight A, et al. Mutation of the gene encoding cellular retinaldehyde-binding protein in autosomal recessive retinitis pigmentosa. *Nat Genet*. 1997;17:198–200.
5. Xue Y, Shen SQ, Jui J, et al. CRALBP supports the mammalian retinal visual cycle and cone vision. *J Clin Invest*. 2015;125:727–738.
6. Burstedt M, Jonsson F, Köhn L, et al. Genotype-phenotype correlations in Bothnia dystrophy caused by RLBP1 gene sequence variations. *Acta Ophthalmol*. 2013;91:437–444.
7. Dessalces E, Bocquet B, Bourien J, et al. Early-onset foveal involvement in retinitis punctata albescens with mutations in RLBP1. *JAMA Ophthalmol*. 2013;131:1314–1323.
8. Collin RWJ, van den Born LI, Klevering BJ, et al. High-resolution homozygosity mapping is a powerful tool to detect novel mutations causative of autosomal recessive RP in the Dutch population. *Invest Ophthalmol Vis Sci*. 2011;52:2227–2239.
9. Eisenberger T, Neuhaus C, Khan AO, et al. Increasing the yield in targeted next-generation sequencing by implicating CNV analysis, non-coding exons and the overall variant load: the example of retinal dystrophies. *PLoS One*. 2013;8:e78496.
10. Nakamura M, Lin J, Ito Y, Miyake Y. Novel mutation in RLBP1 gene in a Japanese patient with retinitis punctata albescens. *Am J Ophthalmol*. 2005;139:1133–1135.
11. Naz S, Ali S, Riazuddin SA, et al. Mutations in RLBP1 associated with fundus albipunctatus in consanguineous Pakistani families. *Br J Ophthalmol*. 2011;95:1019–1024.
12. Demirci FYK, Rigatti BW, Mah TS, Gorin MB. A novel compound heterozygous mutation in the cellular retinaldehyde-binding protein gene (RLBP1) in a patient with retinitis punctata albescens. *Am J Ophthalmol*. 2004;138:171–173.
13. Fishman GA, Roberts MF, Derlacki DJ, et al. Novel mutations in the cellular retinaldehyde-binding protein gene (RLBP1) associated with retinitis punctata albescens: evidence of interfamilial genetic heterogeneity and fundus changes in heterozygotes. *Arch Ophthalmol*. 2004;122:70–75.
14. Hipp S, Zobor G, Glöckle N, et al. Phenotype variations of retinal dystrophies caused by mutations in the RLBP1 gene. *Acta Ophthalmologica*. 2015;93:e281–e286.
15. Morimura H, Berson EL, Dryja TP. Recessive mutations in the RLBP1 gene encoding cellular retinaldehyde-binding protein in a form of retinitis punctata albescens. *Invest Ophthalmol Vis Sci*. 1999;40:1000–1004.
16. Littink KW, van Genderen MM, van Schooneveld MJ, et al. A homozygous frameshift mutation in LRAT causes retinitis punctata albescens. *Ophthalmology*. 2012;119:1899–1906.
17. Chen Z-J, Lin K-H, Lee S-H, et al. Mutation spectrum and genotype-phenotype correlation of inherited retinal dystrophy in Taiwan. *Clin Exp Ophthalmol*. 2020;48:486–499.
18. Wang L, Zhang J, Chen N, et al. Application of whole exome and targeted panel sequencing in the clinical molecular diagnosis of 319 Chinese families with inherited retinal dystrophy and comparison study. *Genes*. 2018;9:360.

19. Al-Bdour M, Pauleck S, Dardas Z, et al. Clinical heterogeneity in retinitis pigmentosa caused by variants in RP1 and RLBP1 in five extended consanguineous pedigrees. *Mol Vis*. 2020;26: 445−458.
20. Martin-Merida I, Avila-Fernandez A, Del Pozo-Valero M, et al. Genomic landscape of sporadic retinitis pigmentosa: findings from 877 Spanish cases. *Ophthalmology*. 2019;126: 1181−1188.
21. Bocquet B, Marzouka NAD, Hebrard M, et al. Homozygosity mapping in autosomal recessive retinitis pigmentosa families detects novel mutations. *Mol Vis*. 2013;19: 2487−2500.
22. Bagheri S, Pantrangi M, Sodhi SK, et al. A novel large homozygous deletion in the cellular retinaldehyde-binding protein gene (RLBP1) in a patient with retinitis punctata albescens. *Retin Cases Brief Rep*. 2020;14:85−89.
23. Humbert G, Delettre C, Sénéchal A, et al. Homozygous deletion related to Alu repeats in RLBP1 causes retinitis punctata albescens. *Invest Ophthalmol Vis Sci*. 2006;47:4719−4724.
24. Richards S, Aziz N, Bale S, et al. Standards and guidelines for the interpretation of sequence variants: a joint consensus recommendation of the American College of Medical Genetics and Genomics and the Association for Molecular Pathology. *Genet Med*. 2015;17:405−424.
25. Pons J-L, Labesse G. @TOME-2: a new pipeline for comparative modeling of protein-ligand complexes. *Nucleic Acids Res*. 2009;37:W485−W491.
26. Canutescu AA, Shelenkov AA, Dunbrack RL. A graph-theory algorithm for rapid protein side-chain prediction. *Protein Sci*. 2003;12:2001−2014.
27. Wu Z, Hasan A, Liu T, et al. Identification of CRALBP ligand interactions by photoaffinity labeling, hydrogen/deuterium exchange, and structural modeling. *J Biol Chem*. 2004;279: 27357−27364.
28. Pawlicka K, Kalathiya U, Alfaro J. Nonsense-mediated mRNA decay: pathologies and the potential for novel therapeutics. *Cancers*. 2020;12:765.
29. Popp MW, Maquat LE. Nonsense-mediated mRNA decay and cancer. *Curr Opin Genet Dev*. 2018;48:44−50.
30. Seko Y, Iwanami M, Miyamoto-Matsui K, et al. The manner of decay of genetically defective EYS gene transcripts in photoreceptor-directed fibroblasts derived from retinitis pigmentosa patients depends on the type of mutation. *Stem Cell Res Ther*. 2018;9:279.
31. He X, Lobsiger J, Stocker A. Bothnia dystrophy is caused by domino-like rearrangements in cellular retinaldehyde-binding protein mutant R234W. *Proc Natl Acad Sci U S A*. 2009;106:18545−18550.